

Gaussian Boson Sampling with Pseudo-Photon-Number Resolving Detectors and Quantum Computational Advantage

Yu-Hao Deng,^{1,2,3} Yi-Chao Gu,^{1,2,3} Hua-Liang Liu,^{1,2,3} Si-Qiu Gong,^{1,2,3} Hao Su,^{1,2,3} Zhi-Jiong Zhang,^{1,2,3} Hao-Yang Tang,^{1,2,3} Meng-Hao Jia,^{1,2,3} Jia-Min Xu,^{1,2,3} Ming-Cheng Chen,^{1,2,3} Han-Sen Zhong,^{1,2,3} Jian Qin,^{1,2,3} Hui Wang,^{1,2,3} Li-Chao Peng,^{1,2,3} Jiarong Yan,^{1,2,3} Yi Hu,^{1,2,3} Jia Huang,⁴ Hao Li,⁴ Yuxuan Li,⁵ Yaojian Chen,⁵ Xiao Jiang,^{1,2,3} Lin Gan,⁵ Guangwen Yang,⁵ Lixing You,⁴ Li Li,^{1,2,3} Nai-Le Liu,^{1,2,3} Jelmer J. Renema,⁶ Chao-Yang Lu,^{1,2,3,7} and Jian-Wei Pan^{1,2,3}

¹Hefei National Laboratory for Physical Sciences at Microscale and School of Physical Sciences,
University of Science and Technology of China, Hefei, Anhui, 230026, China

²CAS Centre for Excellence and Synergetic Innovation Centre in Quantum Information and Quantum Physics,
University of Science and Technology of China, Shanghai, 201315, China

³Hefei National Laboratory, University of Science and Technology of China, Hefei 230088, China
⁴State Key Laboratory of Functional Materials for Informatics,
Shanghai Institute of Micro system and Information Technology (SIMIT),
Chinese Academy of Sciences, 865 Changning Road, Shanghai, 200050, China

⁵Department of Computer Science and Technology and Beijing National Research

Center for Information Science and Technology, Tsinghua University, Beijing, China

⁶Adaptive Quantum Optics Group, Mesa+ Institute for Nanotechnology,
University of Twente, P.O. Box 217, 7500 AE Enschede, Netherlands

⁷New Cornerstone Science Laboratory, Shenzhen 518054, China

We report new Gaussian boson sampling experiments with pseudo-photon-number-resolving detection, which register up to 255 photon-click events. We consider partial photon distinguishability and develop a more complete model for characterization of the noisy Gaussian boson sampling. In the quantum computational advantage regime, we use Bayesian tests and correlation function analysis to validate the samples against all current classical mockups. Estimating with the best classical algorithms to date, generating a single ideal sample from the same distribution on the supercomputer *Frontier* would take ~ 600 years using exact methods, whereas our quantum computer, *Jiǔzhāng* 3.0, takes only $1.27\text{ }\mu\text{s}$ to produce a sample. Generating the hardest sample from the experiment using an exact algorithm would take *Frontier* $\sim 3.1 \times 10^{10}$ years.

Quantum computational advantage (QCA) [1–5] marks an important milestone in the development of quantum computers. By solving certain quantum sampling problems [6, 7] that are intractable for classical supercomputers, QCA experiments [8–12] have provided strong evidence for the long-anticipated quantum speed-up theoretically conceived ~ 40 years ago. Similar to Bell tests [13] which were designed to refute the local hidden variable theories [14], these QCA experiments could be interpreted as violations of the Extended Church-Turing thesis [1].

Interestingly, these QCA experiments have motivated growing study of faster classical simulations [15–19], competing classical spoofing strategies [19–24], and new methods for validation and characterization [25–28]. For example, new classical algorithms [17–19] were put forward which could reduce the classical simulation overhead of Gaussian boson sampling (GBS) [29, 30] by orders of magnitudes lower than brute-force algorithms. Furthermore, newly designed spoofing strategies exploit optimized classical light sources which have higher fidelity with the target squeezed state and thus could produce mockup samples closer to the quantum samples [12]. Additionally, heuristic classical samplers have been conceived to approximate the GBS by means of low-order marginal probabilities or the circuit structure [22, 23].

In return, these new challenges from the classical counterparts motivate the development of higher-fidelity and larger-scale quantum computers as well as a better modeling and

understanding of the increasingly complex system [31–42], which is a fundamental endeavor in its own right [43–45]. Indeed, only by such a continuous quantum-classical competition can the QCA milestone be progressively better established. In this direction, we report in this *Letter* a new, higher-efficiency GBS machine with up to 255 photon clicks in the output using pseudo-photon-number-resolving detectors. A new model is used to characterize the system and validate the samples against all the emerging classical challenges. The computational complexity of this new GBS device, *Jiǔzhāng* 3.0, is analyzed and a new QCA frontier is established.

The first GBS experiments [9, 10] in the QCA regime used threshold detectors to register the samples. In those cases, there was a possibility of photon collision, that is, the photons can bunch at the outputs. New classical algorithms [19] could exploit the photon collision to reduce the simulation overhead. A recent work [12] has reported time-bin-encoded GBS with photon-number resolved detection, in a fiber loop-based configuration similar to an earlier single-photon boson sampling experiment [46]. However, the relatively high photon loss in the fiber loops has allowed only three loops in the implementation, restricting the depth and universality of the interferometer. Additionally, the long recovery time of the transition-edge sensors could render it an unsuitable choice for high-repetition rate experiments.

A schematic of our GBS experiment is shown in Fig. 1. Transform-limited laser pulses double pass periodically poled

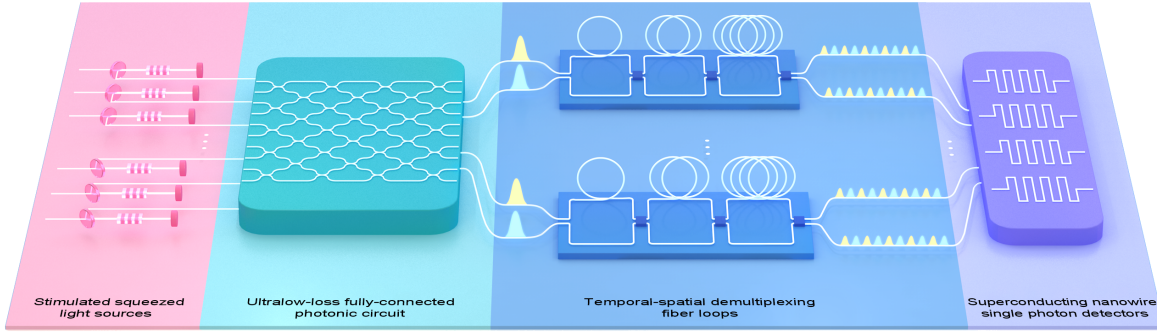


FIG. 1. The experimental setup. 25 stimulated two-mode squeezed state photon sources are all phase-locked to each other and sent into a 144-mode ultralow-loss fully-connected optical interferometer. The photons go through the fiber loops for temporal-spatial demultiplexing and are detected by the superconducting nanowire single photon detectors, which together constitute the pseudo-photon-number resolving detection scheme. Each fiber loop setup includes two input modes as represented by distinct colors. Photons from each mode are temporally demultiplexed by the fiber beam splitters and the delay lines into four time bins, and each time bin is furthermore split into two path bins at the last fiber beam splitter. Polarization-maintaining fiber is implemented for unifying the polarization of all the time bins and path bins. The photons corresponding to each of the two input modes of the fiber loop setup can be distinguished by their parity in time bin with a coincidence event analyzer (not shown).

potassium titanyl phosphate (PPKTP) crystals to create 25 pairs of two-mode squeezed state (TMSS) by a stimulated emission process [10]. The TMSSs have an average efficiency of 88.4% and photon indistinguishability of 96.2%, simultaneously. In the experiment, the laser power is tuned to generate different squeezing parameters ranging from 1.2 to 1.6. The TMSSs are then fed into an ultralow-loss three-dimensional interferometer with full connectivity among all 144 modes. The transmission rate of the interferometer is 97% for each mode, and the average wave-packet overlap inside the interferometer is above 99.5%. The whole set-up is actively phase locked within a precision of 15 nm.

For detection, we implement pseudo-photon number resolution using one-to-eight demultiplexing of the optical modes. The 144 output modes are partitioned into 72 subgroups. Each subgroup is sent through a cascaded fiber-loop element, and split into 16 individual bins separated in time and path (see Fig. 1). Photons from two modes of the same group share two superconducting nanowire single-photon detectors and can be distinguished according to their time bin's parity. The minimal time delay of the fiber loop is 52 ns, longer than the recovery time of the detectors. The capability to resolve the photon number is enabled by temporal and spatial de-multiplexing of the detection events.

We conduct detector tomography [47] of each mode to validate the pseudo-photon-number-resolved detection (PPNRD) scheme[48]. As shown in Fig. S1(a), the probability of the nine photon-click number response of the PPNRD agree well with the theoretical model. The positive-operator valued measures of the nine photon-click number measurement can be constructed from the data, which is shown in Fig. S1(c), together with its Wigner function and fidelity with the theoretical prediction. The PPNRD scheme overcomes the shortcoming of threshold detection that it is incapable of resolving photon-number information, and significantly increases

the sampling task's computational complexity, as we describe later.

While we model the experiment with the PPNRD detection scheme in following discussions, we address the question of how well our detection scheme emulates true photon number-resolving detection here. We first estimate the overall number of photons not detected due to the remaining threshold nature of the individual bins. By computing the photon number probability of the state and the combinatorics of optical loss and threshold detection, we estimate that on average 10 photons are not detected due to this effect at the highest squeezing power utilized in our experiment. While it is currently still an open question whether missed counts due to threshold detection can be used to speed up approximate simulation, we note that this fraction of lost photons is now far below the linear loss in our experiment.

Looking at the problem on the level of individual optical modes, it follows from considerations of combinatorics that PPNRD approaches true photon number resolving detection in the limit where $\langle n \rangle^2 \ll N_{\text{bins}}$, where $\langle n \rangle$ is the mean photon number detected on each mode, and N_{bins} is the number of bins into which each mode is multiplexed ($N_{\text{bins}} = 8$ in our case). For the highest photon density achieved, on average for each port we have $\langle n \rangle^2 = \left(\frac{255}{144}\right)^2 \approx 3.13$, showing that each individual photon detector well approximates a PNR detector in the photon density regime at which our experiment operates.

The overall linear efficiency of the whole experimental set-up is 43%, including the quantum light sources, transmission, and detection. This efficiency is much higher than that in ref. [12], which was 33% although involving only three loops. The photon-click number distribution under three laser powers is shown in Fig. 2(a). The maximum photon-click number reaches 255, which is higher than all the previous GBS experiments.

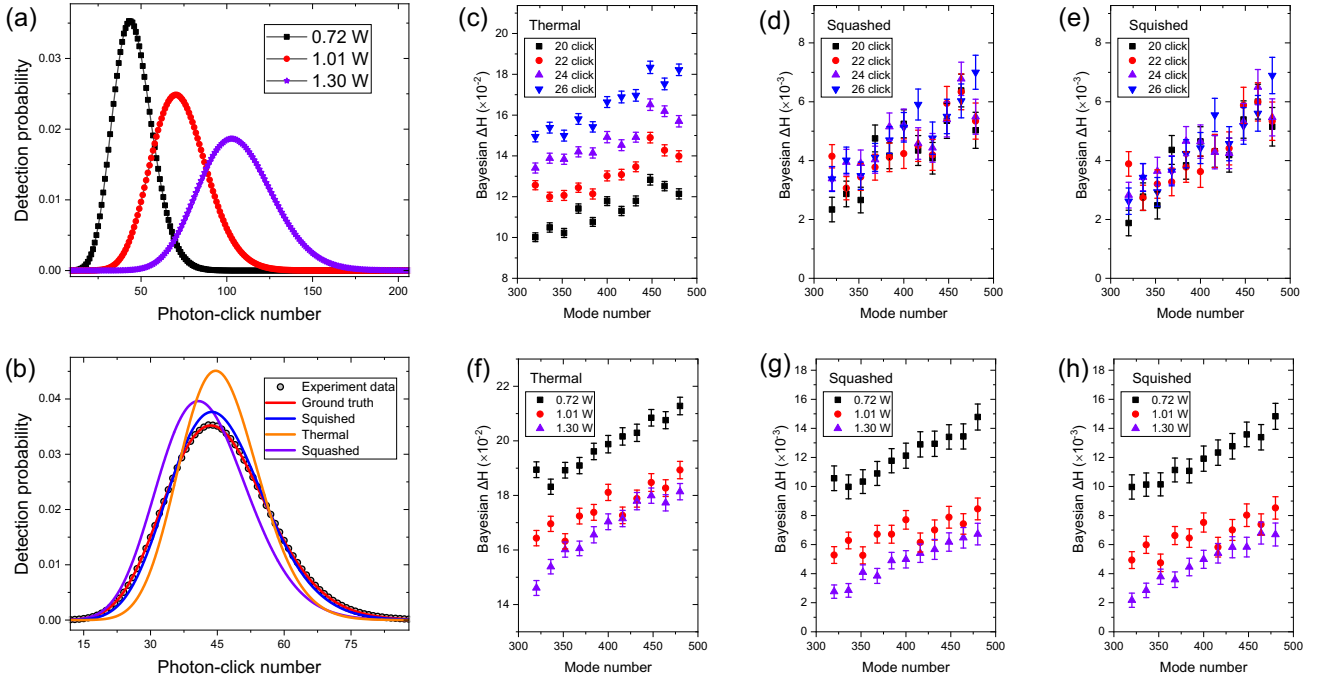


FIG. 2. The experimental photon-click number distribution and the Bayesian validation results. (a) Photon-click number distribution of this work. Data from experiments of three pump laser power ranging from 0.72 W and 1.30 W are displayed. A maximum photon-click number of 129, 203 and 255 are registered for each of the experiments. (b) Photon-click number distribution of the experimental results, the ground-truth theory, the squashed state, the squashed state and the thermal state mockups for the lowest laser intensity configuration. (c), (d), (e) Bayesian confidence of the ground-truth theory as a function of subsystem size, against the thermal state (c), the squashed state (d) and the squished state (e) hypothesis. It can be observed that as the subsystem size grows, the Bayesian confidence is above zero and exhibits a clear increasing trending, indicating an exclusion of the three mockups and a stronger Bayesian confidence for the full system. Bayesian results for photon click number changing from 20 to 26 are displayed in datapoints of different colors and show similar results. (f), (g), (h) Bayesian confidence of the ground-truth theory as a function of the subsystem size for experiments of the three distinct pump laser power. The results show the Bayesian results against the thermal state (f), the squashed state (g) and the squished state (h) hypothesis, for a fixed photon-click number (25). For all pump laser powers, the Bayesian ΔH is above zero and exhibits a clear increasing trending with subsystem size, implying stronger Bayesian confidence for the full system. In all plots error bars indicate standard error. For results of each mode number, the Bayesian score are obtained by averaging over an ensemble of randomly selected subsystems.

We analyze the obtained GBS samples and validate them against known classical hypotheses in the QCA regime. The most powerful methods to spoof the GBS is to use classical states which can maximally approximate the quantum light sources in the experimental set-up with photon loss. Under photon loss, the input squeezed states can be gradually degraded into squeezed thermal states [31]. Thus, in this work, in addition to the thermal state hypothesis which has been tested in *Jiǔzhāng* 1.0 and 2.0, we consider two more competitive hypotheses using squeezed thermal states. The first one is first proposed in ref. [12, 31] and called a squashed state, which is a classical mixture of coherent states and has vacuum fluctuations in one quadrature and larger fluctuation in the other. The squashed states can have a different mean photon number than the squeezed states in order to maximize the fidelity with the quantum light. The second one is similar to the squashed state, but has the constraint that the mean photon number should be the same as the input lossy squeezed state [49], which we call a squished state. Note that there are other

plausible hypotheses such as using coherent light and distinguishable photons, which are much easier to be ruled out. As shown in [48], the validation strength against the other hypotheses is typically 2-4 orders of magnitude larger than the squashed and squished states. Therefore, we will focus on the discussion of the latter in the main text.

We start by comparing the experimental photon number distribution with the ground-truth model and the possible mockups in Fig. 2(b). The GBS data set taken at 0.72 W laser power (dot) well overlaps with the ground truth (red), while obviously deviates from the classical mockups based on the thermal state (yellow), the squished state (purple) and the squashed state (blue). Then, we continue with a more quantitative validation for each output photon number data set. First, we use a Bayesian test [50], where two hypothetical theoretical models are compared against each other for a closer description of the experimental samples. We define the Bayesian test score ΔH as the difference between the ground-truth model H_0 and the classical adversary model hypothesis H_1

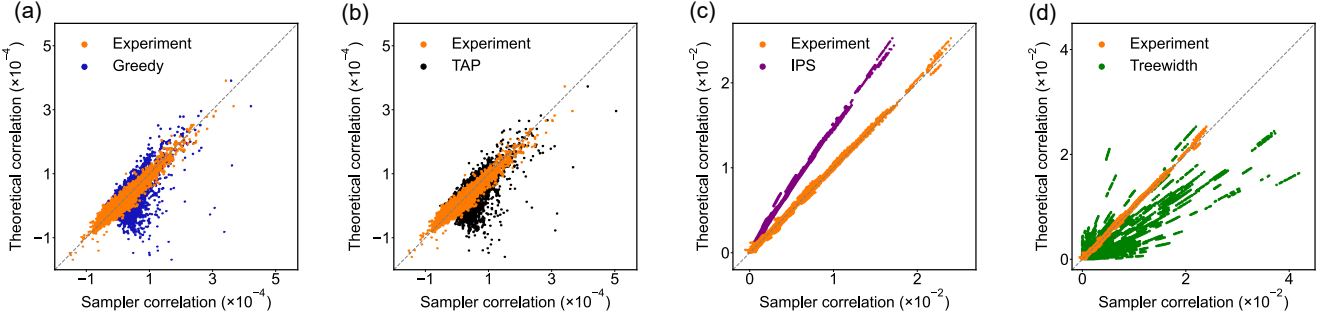


FIG. 3. Correlation function analysis. (a) 3-order correlation function in scatter plot showing the experimental and the greedy sampler in comparison versus the ground-truth theory. (b) Scatter points showing the 3-order correlation function of the experiment and the TAP sampler versus that predicted by the ground-truth theory. For (a) and (b), 10 million samples from the highest pump laser power experiment are used for estimation of the experimental and mockup's correlation. All 3-order correlation functions of 144 out of 1152 modes (1 from each 1-to-8 fan-out modes) are displayed. (c)-(d) Scatter plot of the 2-order correlation function of the experiment and the IPS sampler (c), the treewidth sampler (d), versus the ground-truth theory. In (c)-(d), all pairs of 1152 modes are displayed, and 10 million samples from the highest pump laser power experiment are used for estimation of the experimental correlation whereas exactly theoretical value is used for the mockup samplers. The results clearly exhibit that the ground-truth model is closer to the experimental sampler rather than the classical mockup samplers in the statistical feature of the second or third order correlation function.

on a set of n -photon-click samples:

$$\Delta H = \frac{1}{N} \ln \prod_{i=1}^N \frac{P^{(0)}(\vec{s}_i)P^{(1)}(n)}{P^{(1)}(\vec{s}_i)P^{(0)}(n)} \quad (1)$$

where N is the number of samples, \vec{s}_i represents the i th sample, $P^{(0/1)}(\vec{s}_i)$ represents the event probability of sample \vec{s}_i under the $H_{0/1}$ hypothesis, and $P^{(0/1)}(n)$ is the coarse-grained probability for the n -photon-click under hypothesis $H_{0/1}$. When $\Delta H > 0$, it is proven that the experimental samples are more likely from the ground-truth GBS rather than the mockup. A higher Bayesian test score indicates a larger confidence.

For the validation, each of the 144 modes is treated as 1-to-8 fan out, yielding a total mode number of 1152. Further, in our model we consider the noise of the partial photon indistinguishability for the Bayesian test, where the probability of the sample event is calculated by a modified version of the Torontonian [48]. We find that our model gives a closer description of the experiment than the previous ones. We use the *Sunway TaihuLight* supercomputer to calculate the probability of large photon number samples in the QCA regime.

The Bayesian test score of the ground truth against the mockups using the thermal state, the squashed state, and the squished state at 1.3 W pump power are shown in Fig. 2(c)-2(e). Due to the classical computational overhead, we first start from a subsystem with fewer output bosonic modes, and gradually increase the subsystem size. We observe not only all the Bayesian scores in Fig. 2(c)-2(e) are higher than zero, but also they show an evident increasing trend as the subsystem size ramps up from 300 to 500 for photon-click number between 20 and 26. The positive scores demonstrate that the experimental GBS samples are more likely generated from the ground-truth distribution rather than these mockup distributions. More importantly, the rising trend of the Bayesian score

indicates a higher score can be inferred for the full system, which agrees with the intuition that as fewer modes are traced out, a larger-size subsystem can be validated more strongly. Therefore, we conclusively infer that for the full-mode system, though it is not directly computable, a stronger Bayesian confidence for the ground-truth theory is expected.

We continue to investigate the power dependence of the Bayesian test. In Fig. 2(f)-2(h), the Bayesian validation strength is plotted for three different pump laser powers from 0.72 W to 1.3 W. The results show that the lower pump power can generate higher Bayesian score. This is expected because the thermal noise and photon loss become increasingly sensitive with larger squeezing parameters [51].

Another important tool for characterizing the GBS is the correlation function. The k -order correlation function is recursively defined as

$$\kappa(X_1 X_2 \cdots X_k) = E(X_1 X_2 \cdots X_k) - \sum_{p \in P_k} \prod_{b \in p} \kappa[(X_i)_{i \in b}] \quad (2)$$

where X_k represents the experimental measurement operator at the k th output mode, and P_k represent all partitions of the set $\{1, 2, \dots, k\}$ excluding the universal set. Based on the correlation function, we validate our experimental samples against other recently proposed mockups based on approximating the experimental GBS through low-order marginal distributions [22].

Reference [22] proposed a greedy algorithm to sample from a distribution that approximates all first- and second-order correlations of the experiment, which we call a greedy sampler below. The same work also used the single-mode marginals and two-mode correlations to configure a Boltzmann machine for sampling under the Thouless, Anderson, and Palmer (TAP) mean field approximation. These methods can be generalized to higher orders in principle, but a full enumeration of all the

marginal probabilities of the chosen order is required, which grow combinatorically, and thus limits it within the low-order regime. However, these mockups do not capture higher-order correlations, and can thus be ruled out from this aspect.

In Fig. 3(a)-3(b), we directly compare the third-order correlation functions between the experimental samples at the QCA regime and the mockup samplers from the order-2 greedy and the order-2 TAP samplers. The statistics of the experimental samples agree with the ground truth where they cluster around the identity line at 45° , whereas the mockup samplers' third-order correlations show significant divergence from the ground-truth predictions.

Additionally, ref. [19] designed an Independent Pairs and Singles (IPS) sampler, which generates samples through a procedure composed of many independently single-photon and pair-photon generation processes. The sampler was shown to yield higher heavy output generation score than the mockups using the thermal states and distinguishable photons. We compare the second-order cumulants of the sampler with the experimental results in Fig. 3(c), where the IPS sampler shows an evident deviation from the results of the ground truth and the experimental data.

The last mockup to be ruled out is by considering the local connectivity of the circuits to reduce the overhead of classical approximate sampling [23], which we call treewidth sampler. The sampler could generate higher heavy output generation score than some GBS experiments, which, however, is due to the limitation of heavy output generation itself. In fact, one can show that the treewidth mockup sampler can even yield a higher heavy output generation score than that based on the ideal ground truth [48]. Thus, it is necessary to rule out the treewidth mockup in other ways. In Fig. 3(d), we show the second-order correlation of a treewidth mockup (with a propagation length of 65) and the experimental sampler. The former deviates significantly from the ground-truth theory, and is thus unambiguously ruled out.

Having excluded all currently proposed mockups, we now benchmark the classical computational cost to simulate a noiseless version of our GBS experiment. Our pseudo-photon number resolving detection scheme can be modelled by treating all the 1152 fan-out bins as individual output modes, each with threshold detection. We can use results from [19] to exploit the fact that different output bins corresponding to the same optical mode result in repeated entries in the loop hafnian during the simulation, further reducing the dominant computational cost to:

$$T(\vec{N}) = \frac{1}{2} C_{\text{Frontier}} M N^3 G^{N/2} \quad (3)$$

where $\vec{N} = \{n_1, n_2, \dots, n_{144}\}$ represents the PPNRD sample with n_i being the photon-click number of the i th mode, N is the number of clicked modes, M is the mode number, $G = (\prod_i^M (n_i + 1))^{1/N}$, and C_{Frontier} is estimated based on [12]. The addition of PPNRD therefore substantially increases the computational complexity of our experiment compared to

threshold detection (which always has $G = 2$), due to the strong increase in the number of registered detection events.

We now estimate the time cost on *Frontier*, currently the most powerful supercomputer. For each sample of our experiment, we estimate it would on average take *Frontier* at least ~ 600 years to generate using the exact methods, while it only takes our machine $1.27 \mu\text{s}$ to produce a sample, showing an overwhelming QCA of 1.5×10^{16} . Moreover, the hardest sample from our experiment would take *Frontier* more than $\sim 3.1 \times 10^{10}$ years to generate using exact algorithm. We hope future work will further consider the realistic experimental noise such as photon loss and partial distinguishability for a better benchmark.

We thank Z.-M. He, R.-X. Wang, X.-Y. Wu, Z.-M. Zhang and S.-T. Zheng for helpful assistance during the experiment. We thank Y. Liang and Q.-H. Shi for their help in preparation of the manuscript. This work was supported by the National Natural Science Foundation of China, the National Key R&D Program of China (2019YFA0308700), the Chinese Academy of Sciences, the Anhui Initiative in Quantum Information Technologies, the Science and Technology Commission of Shanghai Municipality(2019SHZDZX01), the Innovation Program for Quantum Science and Technology (No. ZD0202010000), the New Cornerstone Science Foundation, and NWO Veni.

Y.-H. D., Y.-C. G., H.-L. L., S.-Q. G. and H. S. contributed equally to this work.

- [1] E. Bernstein and U. Vazirani, in *Proceedings of the Twenty-Fifth Annual ACM Symposium on Theory of Computing - STOC '93* (ACM Press, San Diego, California, United States, 1993) pp. 11–20.
- [2] J. Preskill, arXiv:1203.5813 (2012).
- [3] A. W. Harrow and A. Montanaro, *Nature* **549**, 203 (2017).
- [4] A. P. Lund, M. J. Bremner, and T. C. Ralph, *npj Quantum Information* **3**, 15 (2017).
- [5] D. Hangleiter and J. Eisert, arXiv:2206.04079 (2023).
- [6] S. Aaronson and A. Arkhipov, in *Proceedings of the 43rd Annual ACM Symposium on Theory of Computing - STOC '11* (ACM Press, New York, New York, USA, 2011) pp. 333–342.
- [7] S. Boixo, S. V. Isakov, V. N. Smelyanskiy, R. Babbush, N. Ding, Z. Jiang, M. J. Bremner, J. M. Martinis, and H. Neven, *Nature Physics* **14**, 595 (2018).
- [8] F. Arute, K. Arya, R. Babbush, D. Bacon, J. C. Bardin, *et al.*, *Nature* **574**, 505 (2019).
- [9] H. S. Zhong, H. Wang, Y. H. Deng, M. C. Chen, L. C. Peng, *et al.*, *Science* **370**, 1460 (2021).
- [10] H.-S. Zhong, Y.-H. Deng, J. Qin, H. Wang, M.-C. Chen, *et al.*, *Physical Review Letters* **127**, 180502 (2021).
- [11] Y. Wu, W.-S. Bao, S. Cao, F. Chen, M.-C. Chen, *et al.*, *Physical Review Letters* **127**, 180501 (2021).
- [12] L. S. Madsen, F. Laudenbach, M. F. Askarani, F. Rortais, T. Vincent, J. F. F. Bulmer, *et al.*, *Nature* **606**, 75 (2022).
- [13] J. S. Bell, *Physics Physique Fizika* **1**, 195 (1964).
- [14] A. Einstein, B. Podolsky, and N. Rosen, *Physical Review* **47**, 777 (1935).
- [15] E. Pednault, J. A. Gunnels, G. Nannicini, L. Horesh, and

R. Wisnieff, arXiv:1910.09534 (2019).

[16] F. Pan, K. Chen, and P. Zhang, *Physical Review Letters* **129**, 090502 (2022).

[17] Ágoston Kaposi, Z. Kolarovszki, T. Kozsik, Z. Zimborás, and P. Rakyta, arXiv:2109.04528 (2022).

[18] N. Quesada, R. S. Chadwick, B. A. Bell, J. M. Arrazola, T. Vincent, H. Qi, and R. García-Patrón, *PRX Quantum* **3**, 010306 (2022).

[19] J. F. F. Bulmer, B. A. Bell, R. S. Chadwick, A. E. Jones, D. Moise, *et al.*, *Science Advances* **8**, eabl9236 (2022).

[20] X. Gao, M. Kalinowski, C.-N. Chou, M. D. Lukin, B. Barak, and S. Choi, arXiv:2112.01657 (2021).

[21] F. Pan and P. Zhang, *Physical Review Letters* **128**, 030501 (2022).

[22] B. Villalonga, M. Y. Niu, L. Li, H. Neven, J. C. Platt, V. N. Smelyanskiy, and S. Boixo, arXiv:2109.11525 (2022).

[23] C. Oh, Y. Lim, B. Fefferman, and L. Jiang, arXiv:2110.01564 (2022).

[24] C. Oh, L. Jiang, and B. Fefferman, arXiv:2210.15021 (2022).

[25] V. Shchesnovich, *Quantum* **5**, 423 (2021).

[26] A. S. Dellios, M. D. Reid, B. Opanchuk, and P. D. Drummond, arXiv:2211.03480 (2022).

[27] B. Seron, L. Novo, A. Arkhipov, and N. J. Cerf, arXiv:2212.09643 (2022).

[28] T. Giordani, V. Mannucci, N. Spagnolo, M. Fumero, A. Rampini, E. Rodolà, and F. Sciarrino, *Quantum Science and Technology* **8**, 015005 (2023).

[29] C. S. Hamilton, R. Kruse, L. Sansoni, S. Barkhofen, C. Silberhorn, and I. Jex, *Phys. Rev. Lett.* **119**, 170501 (2017).

[30] N. Quesada, J. M. Arrazola, and N. Killoran, *Phys. Rev. A* **98**, 062322 (2018).

[31] H. Qi, D. J. Brod, N. Quesada, and R. García-Patrón, *Physical Review Letters* **124**, 100502 (2020).

[32] J. J. Renema, *Physical Review A* **101**, 063840 (2020).

[33] A. S. Popova and A. N. Rubtsov, arXiv:2106.01445 (2021).

[34] P. D. Drummond, B. Opanchuk, A. Dellios, and M. D. Reid, *Phys. Rev. A* **105**, 012427 (2022).

[35] J. Shi and T. Byrnes, *npj Quantum Information* **8**, 54 (2022).

[36] D. Grier, D. J. Brod, J. M. Arrazola, M. B. d. A. Alonso, and N. Quesada, *Quantum* **6**, 863 (2022).

[37] Y. Lim and C. Oh, arXiv:2211.07184 (2022).

[38] A. Dellios, P. D. Drummond, B. Opanchuk, R. Y. Teh, and M. D. Reid, *Physics Letters A* **429**, 127911 (2022).

[39] J. T. Iosue, A. Ehrenberg, D. Hangleiter, A. Deshpande, and A. V. Gorshkov, arXiv:2209.06838 (2022).

[40] Y. Qiao, J. Huh, and F. Grossmann, arXiv:2210.09915 (2022).

[41] M. Liu, C. Oh, J. Liu, L. Jiang, and Y. Alexeev, *Complexity of Gaussian boson sampling with tensor networks* (2023).

[42] C. Oh, L. Jiang, and B. Fefferman, arXiv:2301.11532 (2023).

[43] S. Rahimi-Keshari, T. C. Ralph, and C. M. Caves, *Physical Review X* **6**, 021039 (2016).

[44] A. Deshpande, B. Fefferman, M. C. Tran, M. Foss-Feig, and A. V. Gorshkov, *Physical Review Letters* **121**, 030501 (2018).

[45] U. Chabaud and M. Walschaers, *Physical Review Letters* **130**, 090602 (2023).

[46] Y. He, X. Ding, Z.-E. Su, H.-L. Huang, J. Qin, C. Wang, *et al.*, *Physical Review Letters* **118**, 190501 (2017).

[47] J. S. Lundeen, A. Feito, H. Coldenstrodt-Ronge, K. L. Pregnell, Ch. Silberhorn, T. C. Ralph, J. Eisert, M. B. Plenio, and I. A. Walmsley, *Nature Physics* **5**, 27 (2009).

[48] See Supplemental Materials.

[49] J. Martínez-Cifuentes, K. M. Fonseca-Romero, and N. Quesada, arXiv:2207.10058 (2022).

[50] M. Bentivegna, N. Spagnolo, C. Vitelli, D. J. Brod, A. Crespi, *et al.*, *International Journal of Quantum Information* **12**, 1560028 (2014).

[51] Deng *et al.*, Gaussian boson sampling under thermal noise (to be published).